

## Diode/magnetic tunnel junction cell for fully scalable matrix-based biochip

F. A. Cardoso,<sup>a)</sup> H. A. Ferreira, and J. P. Conde

*INESC-Microsystems and Nanotechnologies, Rua Alves Redol 9, 1000-029 Lisbon, Portugal and Instituto Superior Técnico, Avenida Rovisco Pais, 1000-029 Lisbon, Portugal*

V. Chu

*INESC-Microsystems and Nanotechnologies, Rua Alves Redol 9, 1000-029 Lisbon, Portugal*

P. P. Freitas and D. Vidal

*INESC-Microsystems and Nanotechnologies, Rua Alves Redol 9, 1000-029 Lisbon, Portugal and Instituto Superior Técnico, Avenida Rovisco Pais, 1000-029 Lisbon, Portugal*

J. Germano, L. Sousa, M. S. Piedade, B. A. Costa, and J. M. Lemos

*Instituto Superior Técnico, Avenida Rovisco Pais, 1000-029 Lisbon, Portugal and INESC-Investigação e Desenvolvimento, Rua Alves Redol 9, 1000-029 Lisbon, Portugal*

(Presented on 31 October 2005; published online 19 April 2006)

Magnetoresistive biochips have been recently introduced for the detection of biomolecular recognition. In this work, the detection site incorporates a thin-film diode in series with a magnetic tunnel junction (MTJ), leading to a matrix-based biochip that can be easily scaled up to screen large numbers of different target analytes. The fabricated  $16 \times 16$  cell matrix integrates hydrogenated amorphous silicon (*a*-Si:H) diodes with aluminum oxide barrier MTJ. Each detection site also includes a U-shaped current line for magnetically assisted target concentration at probe sites. The biochip is being integrated in a portable, credit card size electronics control platform. Detection of 250 nm diameter magnetic nanoparticles by one of the matrix cells is demonstrated. © 2006 American Institute of Physics. [DOI: 10.1063/1.2165148]

Magnetoresistive biochips have been recently introduced for fully integrated biomolecular recognition assays.<sup>1,2</sup> In these assays, target biomolecules are marked with magnetic particles and, subsequently, they are recognized by biomolecular probes immobilized at the surface of the chip over sensing sites. The markers' fringe fields are then detected by magnetoresistive sensors: giant magnetoresistive (GMR) sensors,<sup>3,4</sup> spin valves,<sup>5</sup> magnetic tunnel junctions (MTJs),<sup>6</sup> or planar Hall-effect sensors.<sup>7</sup> However, actual biochips have few sensing elements (25 in the INESC MN cystic fibrosis biochip,<sup>5</sup> 64 sensors in the BARC biochip,<sup>3</sup> and 206 sensors in the biochip developed at the University of Bielefeld<sup>4</sup>).

In order to increase this number and make the present biochips fully scalable, a matrix-based biochip was designed and fabricated. The proposed basic cell consists of a thin-film *a*-Si:H diode (TFD) connected in series with a MTJ (Fig. 1). The MTJ was used due to the flexibility in controlling the MTJ resistance of the sensor by changing the barrier thickness, and also due to its higher sensitivity when compared with spin valve sensors, which enables the detection of smaller labels. The diode switching element was chosen rather than a three-terminal device, such as a transistor, in order to avoid additional control lines. The presented architecture was used previously for magnetic random access memory (MRAM) devices.<sup>8</sup> In this latter case, large diode dimensions ( $200 \times 200 \mu\text{m}^2$ ) were needed to pass the required write currents through the diodes. This was the main reason to prevent the use of this architecture for dense MRAMs. For biochip applications, this is no longer a major limitation since probe sites have yet dimensions of a few

hundred  $\mu\text{m}^2$  (similar to the TFD dimensions), and, for now, the number of immobilized probes will not exceed a few hundreds to a few thousands.

In the present design, the biochip is being integrated in a credit card dimension portable platform that incorporates all the electronics for addressing, reading out, sensing, controlling temperature, and the system for fluid handling. The control of the platform is done through a personal digital assistant (PDA) via a wireless channel or a standard bus.

In the  $16 \times 16$  matrix prototype described here, each TFD and the corresponding MTJ sensor are connected in series and this circuit is driven by a programmed current, provided through a digital-to-analog converter (DAC). The sense current flows through row and column multiplexers according to the address of the cell, establishing a single closed circuit at a time. This allows the use of a single DAC and a single amplifier. The TFD has two main functions that correspond to two different modes of the circuit operation: (i) selecting single cells out of the matrix, by forward biasing the selected cell while all the others are reverse-biased, and

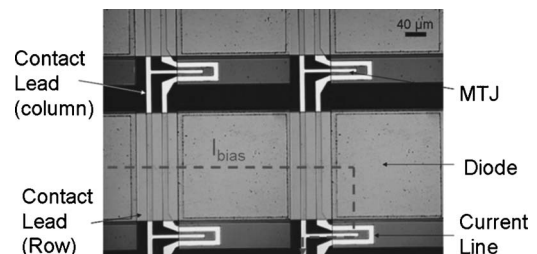


FIG. 1. Top view of four cells of the  $16 \times 16$  matrix. The U-shaped current line structure is designed to sweep the target biomolecules at low frequencies over the immobilized probes (Ref. 5).

<sup>a)</sup>Electronic mail: fcardoso@inesc-mn.pt

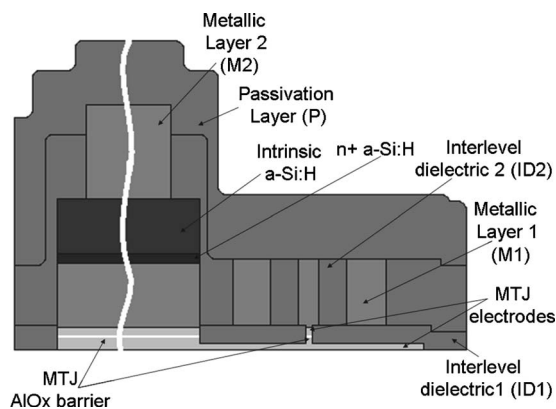


FIG. 2. Cross-sectional view of the biochip showing the MTJ sensor, diode, leads, U-shaped lines, interlevel dielectrics, and passivation layers.

(ii) sensing and controlling the temperature of the probe site to which the diode is allocated. For measuring the signal response of the magnetic tunnel junction sensor, an alternate magnetic field is created by a coil placed below the chip. This signal is precisely generated by the microcontroller/digital signal processor (DSP). Advanced digital signal processing techniques are used to filter signals and to measure the signal originated by the external magnetic field. This processing is equivalent to the lock-in technique used in the laboratory experimental setup.<sup>5</sup>

In addition, each cell includes also a U-shaped current line adjacent to the MTJ (Fig. 1). The superposition of a dc magnetic field created by the current lines with a low-frequency, few hertz, in-plane transversal ac external field leads to attractive magnetic forces that concentrate the magnetic labels in the inner region of the U-shaped line (sensing site). This, in turn, allows much faster (few minutes) hybridization rates between biological targets and the immobilized probes, when compared with diffusion-controlled processes.<sup>9</sup>

In this paper, the fabrication and the working of the basic cell, diode in series with the MTJ, is explained. In addition, the detection of magnetic nanoparticles using this device is shown. Finally, the device response per particle was estimated based on the device and particle characteristics.

Figure 2 shows a detailed cross section of the biochip at a sensing site. The process began by depositing the following MTJ structure on top of a glass substrate: Ta 90 Å/NiFe 50 Å/MnIr 250 Å/CoFeB 50 Å/Al 12 Å (+oxidation)/CoFeB 15 Å/NiFe 45 Å/Ta 30 Å/TiW(N) 150 Å. All the layers were deposited by ion beam in a Nordiko 3000 system. Here NiFe stands for Ni<sub>80</sub>Fe<sub>20</sub>, MnIr for Mn<sub>76</sub>Ir<sub>24</sub>, CoFeB for (Co<sub>80</sub>Fe<sub>20</sub>)<sub>90</sub>B<sub>10</sub>, and TiW for Ti<sub>10</sub>W<sub>90</sub>, all in at. %. The magnetic layers were deposited under a 40 Oe magnetic field to induce parallel easy axis in the pinned and free layers. The oxidation of the Al layer was done with remote Ar/O<sub>2</sub> plasma during 60 s. After junction definition (two ion milling steps), a 500-Å-thick Al<sub>2</sub>O<sub>3</sub> thick layer (ID1) was rf sputtered to laterally isolate the junction. A 2000 Å Al/150 Å TiW(N) (M1) thick layer was then deposited by magnetron sputtering in a Nordiko 7000 system, forming the diode bottom electrode, the column leads, and the U-shaped magnetic-field-generating lines. M1 patterning

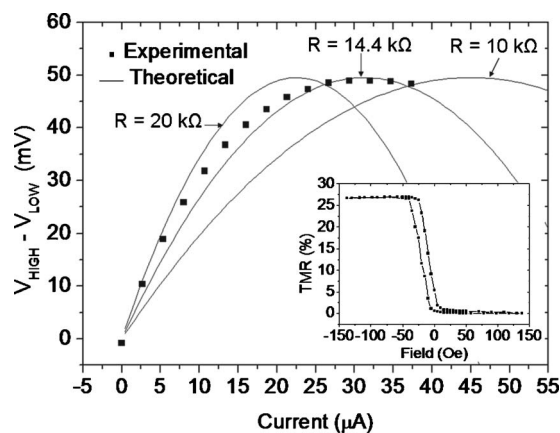


FIG. 3. Experimental and simulated TFD-MTJ response curves vs drive current. The inset shows the transfer curve of a MTJ sensor.

was done by wet etching after removing the TiW(N) layer by ion milling. Diode fabrication proceeded, at 250 °C, with a rf plasma-enhanced chemical-vapor deposition (PECVD) growth of 200 Å n+-a-Si:H (which forms an Ohmic contact with the bottom electrode) and a 2000 Å intrinsic a-Si:H layer.<sup>8</sup> The diode was patterned by reactive ion etching. A second dielectric layer, 2500 Å of Al<sub>2</sub>O<sub>3</sub> (ID2), was deposited by sputtering for the isolation of the columns leads, and vias and contacts were opened by lift-off. The final metallic layer, 3000 Å Al/150 Å TiW(N) (M2), was deposited to form the Schottky barrier and the row leads. Finally, the whole chip was passivated with a 1000 Å Al<sub>2</sub>O<sub>3</sub>/2000 Å SiO<sub>2</sub> (P) layer for protection against corrosion from fluids and to provide a suitable surface for biofunctionalization.<sup>5</sup> The MTJ and diode were patterned down to 2 × 10 μm<sup>2</sup> (MTJ) and 200 × 200 μm<sup>2</sup> (diode) dimensions. The chip was further annealed at 280 °C under a magnetic field of 3 kOe to create an exchange field in the MTJ pinned layer and to reduce diode defects.

For biodetection applications, sensors should have a linear response to external fields. With this in mind, a sensor aspect ratio of 5:1 was chosen such that the shape anisotropy alone would be sufficient to rotate the free layer magnetization into the longer dimension, perpendicular to the pinned layer magnetization. The transfer curve for the MTJ shown in the inset of Fig. 3 still has a non-negligible coercivity (10 Oe) and is nonideal. During experimentation one of the branches of this transfer curve was used. In future runs, crossed easy axis will be used to minimize sensor hysteresis.

The superparamagnetic particles used in the experiments were 250 nm diameter Nanomag®-D, composed of iron oxide (magnetite) dispersed in a dextran matrix (Micromod, Germany). The magnetic moment per label was found to be ~1.6 × 10<sup>-13</sup> emu for a 15 Oe magnetizing field.<sup>1</sup> During magnetic nanoparticle detection experiments, a planar electromagnet was used to create an in-plane 15 Oe rms at 30 Hz+6 Oe dc bias field over the chip. The dc magnetic field is used to saturate the MTJ on the lower-resistance state while the ac field is used to vary from that state into the linear part of one of the branches of the transfer curve and also to magnetize the beads. Direct connections were made to the device (MTJ+diode) and an external lock-in was used

to read out the data shown in this paper. Data analysis with the electronics platform described in Fig. 2 is under test. Small volumes ( $\sim 10 \mu\text{l}$ ) of a magnetic nanoparticle solution ( $\sim 10^{11}$  particles/ml), diluted in 1:10 and 1:100, were used. Before washing the chip with distilled water, the particles were left to settle onto the sensor surface for 10 min.

Individual characterization of the MTJ sensor showed a tunneling magnetoresistance ratio (TMR) of 27% and a resistance of 14.4 k $\Omega$  (Fig. 3). In addition, the diode showed an ON/OFF ratio of  $10^5$  at 1 V, a reverse bias current density ( $J_0$ ) of  $5.35 \times 10^{-7}$  A/cm $^2$  and an ideality factor  $n$  of 1.79, given the diode response  $J = J_0 \exp[eV/(nk_B T)]$ . These values were taken after annealing the sample.

Figure 3 shows the voltage change of the serial device discussed above, when the MTJ changed from the high-resistance to the low-resistance state. Device simulations for three different MTJ resistances (10, 14.4, and 20 k $\Omega$ ) are also shown, and agree well with the experimental curve. The curves show a maximum signal  $\Delta V$  of  $\sim 50$  mV for a drive current of 30  $\mu\text{A}$ . The decrease of  $\Delta V$  for higher biasing currents is caused by the TMR decrease at increasing bias voltage. For biochip applications, a maximum variation on the voltage is required.

Increasing MTJ resistance decreases the current required to maximize signal output but at the expenses of increased sensor noise (mostly  $1/f$  for low-frequency applications), while lowering MTJ resistance (e.g., sensors with larger active area for similar  $R \times A$  values or alternatively sensors with lower  $R \times A$  for the same area) pushes the maximum signal peak to higher currents. For the present TFDs, currents in excess of few hundred  $\mu\text{A}$  will cause irreversible diode damage. So the MTJ area and  $R \times A$  values must be optimized for maximum tolerable current through the diode. Nevertheless, the diode forward bias current can be improved in two orders of magnitude by using microcrystalline Si ( $\mu\text{c-Si}$ ) instead of  $a\text{-Si:H}$ .<sup>10</sup> This means that more current can be applied to the device so that the MTJ resistance can be reduced by decreasing the  $R \times A$  value or increasing the sensitive area. In the present demonstration, MTJ characteristics are defined by the diode.

The response of the device to 250 nm diameter magnetic nanoparticle solutions at two different dilutions is shown in Fig. 4. In this assay, the U-shaped lines were not used. Upon particle settling over the sensor, detection signals of 450 and 650  $\mu\text{V rms}$  were obtained for 10  $\mu\text{L}$  of 1:100 and 1:10 dilutions of a 250 nm particle solution, respectively. A device response of  $\sim 14 \mu\text{V rms/particle}$  for a 15 Oe rms applied field was calculated based on a model previously described.<sup>1</sup> A magnetic moment of  $1.6 \times 10^{-13}$  emu/particle was used<sup>1</sup> and a magnetic dipole approximation was considered, with the dipole located at 1.125  $\mu\text{m}$  above the MTJ free layer (distance between the center of the particle and the free layer). Furthermore, in the calculations a MTJ sensor with a TMR of 27%, a resistance of 14.4 k $\Omega$ , and a sensitivity of 0.73 %/Oe was considered, and a drive current of 30  $\mu\text{A}$  was used.

In conclusion, this paper showed that a device comprising MTJ in series with a TFD can be used for nanoparticle

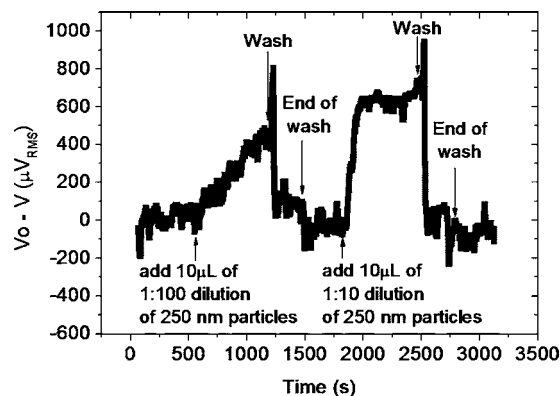


FIG. 4. Device voltage variation to 250 nm nanoparticles at two different dilutions (1:100 and 1:10). Particles were left to settle onto the sensor surface for 10 min before washing the chip with distilled water.

detection and, consequently, could be used for magnetic-label-based bioassays like those previously shown.<sup>1,2</sup> This basic cell enables the fabrication of a fully scalable matrix-based biochip for hundreds to thousands of biological probe sites.

This device can be further improved, though. The sensitive area is still small ( $2 \times 10 \mu\text{m}^2$ ) when compared with conventional probe site areas (few hundred  $\mu\text{m}^2$ ). Although, this limitation can be compensated by the use of U-shaped lines that concentrate particles at sensor,<sup>9</sup> sites' larger area sensors are being developed for increased biological sensitivity. In addition, work is in progress on microcrystalline silicon ( $\mu\text{c-Si}$ ) diodes in order to be able to carry high currents with lower sensor resistances. Furthermore, the TMR of the MTJ can be improved, up to 200%, using MgO barriers instead of  $\text{Al}_2\text{O}_3$  barriers. This will improve the sensitivity of the device to the magnetic markers.

Finally, the biochip is being integrated in a PDA-controlled portable platform that incorporates all the electronics and the microfluidics needed for bio assay applications such as genetic diagnostics and cell detection.

Support is acknowledged to the Portuguese national project POSC/EEA-ESE/58523/2004. One of the authors (H.A.F.) is grateful to FCT for a doctoral grant (SFRH/BD/5031/2001).

<sup>1</sup>P. P. Freitas, H. A. Ferreira, D. L. Graham, L. A. Clarke, M. D. Amaral, V. Martins, L. Fonseca, and J. M. S. Cabral, in *Magneto-electronics*, edited by M. Johnson (Academic, New York, 2004).

<sup>2</sup>D. L. Graham, H. A. Ferreira, and P. P. Freitas, *Trends Biotechnol.* **22**, 455 (2004).

<sup>3</sup>J. C. Rife, M. M. Miller, P. E. Sheehan, C. R. Tamanna, M. Tondra, and L. J. Whitman, *Sens. Actuators, A* **107**, 209 (2003).

<sup>4</sup>J. Schotter, P. B. Kamp, A. Becker, A. Pühler, G. Reiss, and H. Brückl, *Biosens. Bioelectron.* **19**, 1149 (2004).

<sup>5</sup>H. A. Ferreira, D. L. Graham, N. Feliciano, L. A. Clarke, M. D. Amaral, and P. P. Freitas, *IEEE Trans. Magn.* **41**, 4140 (2005).

<sup>6</sup>W. Shen, X. Liu, D. Mazumdar, and G. Xiao, *Appl. Phys. Lett.* **86**, 253901 (2005).

<sup>7</sup>L. Ejsing, M. F. Hansen, A. K. Menon, H. A. Ferreira, D. L. Graham, and P. P. Freitas, *Appl. Phys. Lett.* **84**, 4729 (2004).

<sup>8</sup>R. C. Sousa, P. P. Freitas, V. Chu, and J. P. Conde, *IEEE Trans. Magn.* **35**, 2832 (1999).

<sup>9</sup>H. A. Ferreira, N. Feliciano, D. L. Graham, L. A. Clarke, M. D. Amaral, and P. P. Freitas, *Appl. Phys. Lett.* **87**, 013901 (2005).

<sup>10</sup>Q. Wang *et al.*, *Appl. Phys. Lett.* **85**, 2122 (2004).